Published in final edited form as:
Nat Chem. 2009 May 1; 1: 145–150. doi:10.1038/nchem.162.

A Diiron(IV) Complex that Cleaves Strong C-H and O-H Bonds

Dong Wang, **Erik R. Farquhar**, **Audria Stubna**, **Eckard Münck***, and **Lawrence Que Jr.***
Department of Chemistry and Center for Metals in Biocatalysis, University of Minnesota, Minneapolis, MN, 55455 USA.Department of Chemistry, Carnegie Mellon University, Pittsburgh, PA, 15213 USA

Abstract

The controlled cleavage of strong C-H bonds like those of methane poses a significant challenge for chemists. In nature methane is oxidized to methanol by soluble methane monooxygenase via a diiron (IV) intermediate called Q. To model the chemistry of MMO-Q, an oxo-bridged diiron(IV) complex has been generated by electrochemical oxidation and characterized by several spectroscopic methods. This novel species has an $Fe^{IV/III}$ redox potential of +1.50 V vs. ferrocene (>2 V vs. NHE), the highest value thus far determined electrochemically for an iron complex. This species is quite an effective oxidant. It can attack C-H bonds as strong as 100 kcal mol^{-1} and reacts with cyclohexane a hundred- to a thousand-fold faster than mononuclear Fe^{IV}=O complexes of closely related ligands. Strikingly, this species can also cleave the strong O-H bonds of methanol and *tert*-butanol instead of their weaker C-H bonds, representing the first example of O-H bond activation for iron complexes.

The controlled cleavage of strong C-H bonds like those of methane remains an elusive goal and one of great industrial and practical importance. In nature, methane hydroxylation occurs by oxygen activation through the action of soluble and particulate methane monooxygenases (MMOs) found in methane-metabolizing bacteria[1–4]. The much better characterized soluble MMOs have a nonheme diiron active site that reacts with O_2 to produce an oxo-bridged diiron (IV) oxidant called **Q** that effects the transformation[5–8]. The generation of a diiron(IV) complex that can oxidize strong C-H bonds thus represents an appealing challenge for synthetic chemists.

To date, only two types of (μ-oxo)diiron(IV) complexes have been characterized. The first example, represented by two complexes of tetraamido macrocyclic ligands (TAML) characterized by Ghosh *et al*., is stable at room temperature, but no oxidation chemistry involving C-H bond cleavage has been reported[9]. The second example, recently reported by Xue *et al.*, utilizes the neutral tetradentate N4 ligand tris(3,5-dimethyl-4-methoxy-pyridylmethyl)amine to form $[Fe^{IV}_2(\mu\text{-}O)_2(N4)_2]^{4+}$ and serves as a synthetic precedent for the $Fe^{IV}_2(\mu\text{-}O)_2$ core proposed for MMO-**Q**[10]. This complex is stable for only 1 hour at −40 °C and can attack the weak C-H bonds of dihydroanthracene. These (μ-oxo)diiron(IV) complexes thus exhibit reactivities that fall far short of that associated with the diiron active site of soluble MMO. In this study, we report a much more strongly oxidizing (μ-oxo)diiron(IV) complex, obtained by electrochemical oxidation of its (μ-oxo)diiron(III) precursor, that is capable of cleaving not only the strong C-H bonds of cyclohexane but also the even stronger O-H bonds of aliphatic alcohols.

*To whom correspondence should be addressed. Email: larryque@umn.edu; emunck@cmu.edu.

Author Contributions

D.W., E.M. and L.Q. conceived and designed the experiments; D.W., E.R.F. and A.S. performed the experiments; D.W., E.R.F., A.S. and E.M. analyzed the data; D.W., E.R.F., A.S., E.M. and L.Q. wrote the paper.

All authors discussed the results and commented on the manuscript.

The starting point for this study is $[Fe^{III}_2O(L)_2]^{2+}$ (**1**), a (μ-oxo)diiron(III) complex of L, where L is *N*, *N*-bis-(3′,5′-dimethyl-4′-methoxypyridyl-2′-methyl)-*N*′-acetyl-1,2- diaminoethane. Its structure (Fig. 1a) shows that L acts as a pentadentate ligand with an N_4O donor set where the N_4 subset binds to one iron center while the oxygen atom coordinates to the other iron site. This structure resembles that of a recently described complex of a closely related ligand[11], both of which have a (μ-oxo)diiron(III) unit that is supported by two carboxamido bridges. The fact that the bridging moieties are connected to the terminal ligands results in smaller Fe-(μ-O)-Fe angles than found typically for closely related (μ-oxo)bis(μ-carboxylato)diiron(III) complexes[12], and these (μ-oxo)bis(μ-carboxamido)diiron(III) complexes have the shortest Fe-Fe distances (~3 Å) in this class of complexes.

Cyclic voltammetry (CV) of **1** in CH_3CN at room temperature reveals the presence of two redox waves (Fig. 2a). Scanning anodically from 0 V vs. the ferrocenium/ferrocene couple ($Fc^{+/o}$) elicits an oxidative wave with a peak potential $E_{p,\,a}$ of +1.07 V vs. $Fc^{+/o}$; scan reversal below 1.2 V gives rise to a reductive wave with a peak potential $E_{p,\,c}$ of +0.33 V, which is not observed unless the oxidative wave at +1.07 V is also present. A similarly large separation of the oxidative and reductive waves has been observed by Wieghardt and co-workers in the one-electron oxidation of related (μ-oxo)bis(μ-carboxylato)diiron(III) complexes[13]. Although not strictly reversible by CV criteria (e.g. a ~0.06 V peak separation between $E_{p,\,a}$ and $E_{p,\,c}$), these one-electron redox transformations are reversible by spectropotentiometric and chemical methods. More interestingly, increasing the potential above 1.20 V in the CV experiment on **1** reveals a second redox process (Fig. 2a) with a half-wave potential $E_{1/2}$ of +1.50 V vs. $Fc^{+/o}$; in this case, the separation between the oxidative and reductive waves (ΔE = 0.07 V) approaches that expected for reversible CV behavior. These results suggest that **1** can be oxidized in two one-electron steps to attain a diiron(IV) oxidation state.

Controlled potential bulk electrolysis has been used in this study to prepare sufficient amounts of the oxidized species for detailed spectroscopic characterization. Complex **1** exhibits optical features at 370 nm (ε = 3400 M^{-1} cm^{-1}), 432 nm (ε = 2200 M^{-1} cm^{-1}), 508 nm (ε = 730 M^{-1} cm^{-1}) and 680 nm (ε = 180 M^{-1} cm^{-1}) (Fig. 2b, dotted line), the latter two bands being characteristic of a (μ-oxo)diiron(III) complex with an Fe-O-Fe angle of ~130° [refs. [12,14]]. Electrolysis of **1** at potentials above +0.70 V vs. $Fc^{+/o}$ in CD_3CN at −40 °C produces a dark red species **2** with absorbance maxima at 550 nm (ε = 1800 M^{-1} cm^{-1}) and 878 nm (ε = 770 M^{-1} cm^{-1}) (Fig. 2b, solid line). These features resemble those reported by Wieghardt in the one-electron oxidation of (μ-oxo)bis(μ-carboxylato)diiron(III) complexes to generate iron(III) iron(IV) derivatives[13]. Complex **2** is stable for several days at −40 °C and can be re-reduced to regenerate **1** in quantitative yield either electrochemically by shifting to a potential below +0.70 V or chemically by the addition of one equivalent ferrocene. Thus, the oxidation of **1** to **2** is reversible. Counting charge during the oxidative electrolysis reveals the extraction of one electron from **1**, consistent with the reductive titration. Therefore, ***2 is a one-electron oxidized derivative of 1***.

Increasing the bulk electrolysis potential to +1.70 V after the formation of **2** in CD_3CN at −40 °C affords a black species **3** with no distinct absorption bands (Fig. 2b, dashed line). Complex **3** is much less stable than **2**, but its half-life of ~1 h at −40 °C is long enough to allow its spectroscopic characterization. It is formed in 85% yield, as indicated by Mössbauer spectroscopy (see below) and reductive titration (Fig. 3 inset) where the addition of 0.85 equivalent ferrocene converts **3** to **2**. Therefore, ***3 is a two-electron oxidized derivative of 1***. The time required to accumulate **3** is much longer than that for complete conversion of **1** to **2**, and the yield of **3** can be improved by using CD_3CN instead of CH_3CN as solvent (versus only 30% in CH_3CN) and KPF_6 in place of quaternary ammonium salts as electrolyte, substitutions that minimize the number of potentially oxidizable C-H bonds in the electrolysis medium.

X-ray absorption spectroscopy demonstrates that oxidation of **1** to **2** and **3** occurs at the iron centers. As shown in Fig. 3a and Table 1, the Fe K-edge exhibits a progressive blue shift from **1** to **2** to **3**, the total upshift of 1.5 eV being in accord with a stepwise increase in the oxidation state of the diiron unit in this series. EXAFS analysis (Figs. 3b and S1, Tables 1 and S2–S4) reveals further structural details. For **1,** the respective Fe-N/O and Fe-C distances of 2.11 and 3.07 Å are as expected for the ligand L bound to a high-spin iron(III) center. These distances respectively decrease by 0.15 and 0.2 Å in **2** and **3**, consistent with the iron centers in these complexes undergoing a transition to low spin upon oxidation. There are additional features in the EXAFS analysis assignable to the Fe-O-Fe unit. The Fe-μ-O distance of 1.78 Å of **1** decreases to 1.71 Å in **2** and **3**; the latter distances compare favorably with those of the two crystallographically characterized $[Fe^{IV}_2(O)(TAML)_2]^{2-}$ complexes (1.7284(8) and 1.744(3) Å)[9]. The Fe-Fe distance increases from 2.97 Å for **1** to 3.07 Å for **2** and 3.08 Å for **3**. The changes in Fe-Fe distance are comparable to the 0.05–0.08 Å increase observed upon one-electron oxidation of $[Fe^{III}M^{III}(\mu\text{-}O)(\mu\text{-}O_2CR)_2(Me_3TACN)_2]^{2+}$ (M = Fe or Cr) and $[Fe^{III}Fe^{IV}(\mu\text{-}O)_2(N4)_2]^{3+}$ [refs. [10,13]]. These results strongly suggest that the (μ-oxo)bis(μ-carboxamido)diiron core is maintained upon oxidation (Fig. 1b).

Mössbauer studies also show that oxidation occurs at the iron centers. The 4.2 K zero field Mössbauer spectrum of **1** exhibits a single quadrupole doublet with parameters and high-field behavior typical of an antiferromagnetically coupled (μ-oxo)diiron(III) unit, as expected (Table 1). Upon oxidation to **2** and **3**, the isomer shifts decrease substantially to values near 0 mm s^{-1} (Table 1), indicating that the high-spin iron(III) sites of **1** convert to low-spin iron centers. The corresponding spectrum of **3** (Fig. 4 top) also exhibits a single quadrupole doublet representing 85–90% of the iron in the sample with parameters (ΔE_Q = 2.14 mm s^{-1} and δ = −0.05 mm s^{-1}). These parameters are nearly identical to those of $[Fe^{IV}_2(\mu\text{-}O)_2(N4)_2]^{4+}$ where the individual iron sites are S = 1 [ref. [10]]. The 8.0 T spectra of **3** (Fig. 4 bottom) and $[Fe^{IV}_2(\mu\text{-}O)_2(N4)_2]^{4+}$ both lack paramagnetic hyperfine structure, indicating antiferromagnetic coupling between the two Fe^{IV} sites to provide a dimer ground state with S = 0. Given the likely N_4O_2 ligand set, we assume that the local sites of **3** have $S_1 = S_2 = 1$, in accord with observations of S = 1 ground states for other $Fe^{IV}(N_4O_2)$ complexes[15,16].

Complex **3** has the highest redox potential (+1.50 V vs. $Fc^{+/o}$) among the three types of (μ-oxo)diiron(IV) complexes synthesized thus far, being respectively 1.7 V and 0.7 V more positive than those of $[Fe^{IV}_2(\mu\text{-}O)(TAML)_2]^{2-}$ and $[Fe^{IV}_2(\mu\text{-}O)_2(N4)_2]^{4+}$ [refs. [9,10]]. The redox potential of **3** is also more positive than the value of +0.90 V vs. $Fc^{+/o}$ determined for $[Fe^{IV}(O)(N4Py)]^{2+}$ (N4Py = *N*, *N*-bis(2-pyridylmethyl)-bis(2-pyridyl)methylamine)[17], a complex with a terminal Fe=O unit that has been found to cleave the C-H bonds of cyclohexane[18]. Thus **3** should be quite a powerful oxidant.

Reactivity studies demonstrate that **3** can cleave C-H bonds with $D_{C\text{-}H}$ values as high as 100 kcal mol^{-1}, and the logarithm of the second order rate constants normalized on a per hydrogen basis (log k_2') for these oxidations correlates inversely with the strength of the C-H bonds being cleaved (Fig. 5). In all cases studied, hydrocarbon oxidation results in the quantitative reduction of **3** to **2** (Fig. S2), demonstrating that **3** acts as a one-electron oxidant. Cyclohexane ($D_{C\text{-}H}$ = 99.3 kcal mol^{-1}) is oxidized by **3** with a second order rate constant (k_2) of 8.1×10^{-2} M^{-1} s^{-1} at 10 °C, while the oxidation rate for cyclohexane-d_{12} ($D_{C\text{-}D}$ = 100.6 kcal mol^{-1}) is a factor of 3.5 smaller (Fig. S3). This kinetic isotope effect (KIE) of 3.5 shows that C-H bond cleavage is an important component of the rate determining step. However the observed formation of **2**, but not its conjugate acid, suggests that protonated **2** is quite acidic and readily loses the proton acquired in the H-atom abstraction step.

GC analysis of the products of cyclohexane oxidation under anaerobic conditions shows the formation of cyclohexene and 1,3-cyclohexadiene in respective yields of 13% and 9% (but no

cyclohexanol nor benzene), accounting for 63% of the oxidizing equivalents available in the conversion of **3** to **2** (Table S6). The oxidizing equivalents unaccounted for may be ascribed to the self-decay of **3**, which has a first order rate constant of 0.003 s^{-1}, about a factor of 3 smaller than the pseudo-first-order decay constant of 0.01 s^{-1} observed in the presence of 0.1 M cyclohexane. For comparison, we have also investigated the oxidations of cyclohexene and 1,3-cyclohexadiene by **3** independently under the same experimental conditions as above. Because of their much weaker C-H bonds, these substrates react very rapidly with **3** and quantitatively afford **2** in both reactions. Cyclohexene and 1,3-cyclohexadiene are respectively converted to 1,3-cyclohexadiene and benzene in 47% and 45% yields per diiron(IV) unit, which account for ≥90% of the oxidizing equivalents in each reaction. The absence of hydroxylated products in the reactions above suggests that C-O bond formation after the initial H-abstraction step may be disfavored due to the bridging nature of the oxo atom and the consequent requirement for cleavage of two Fe-O bonds to form the alcohol product. Instead, dehydrogenation occurs either by abstraction of the β-H atom of the alkyl radical by a second diiron(IV) center or by electron transfer from the alkyl radical to another diiron(IV) molecule to generate the cation, followed by loss of a proton from the β-carbon atom[19–21]. Thus **3** acts as a hydrocarbon dehydrogenating agent, rather than as a hydroxylating agent (Fig. 6).

Interestingly, aliphatic alcohols methanol (D_{C-H} = 96.1 kcal mol^{-1}) and *tert*-butanol (D_{C-H} = 100 kcal mol^{-1}) also serve as substrates for oxidation by **3** with respective k_2 values of 0.14 and 0.30 M^{-1} s^{-1}. These values, when normalized on per hydrogen basis, fall well above the line for the linear correlation shown in Fig. 5. Kinetic studies of methanol and *t*-BuOH with different degrees of deuteration (Fig. S4 and S5, respectively) show that changing the C-H bonds to C-D bonds does not affect their respective oxidation rates. However deuteration of the O-H bond results in a KIE of 1.4–1.5. Thus oxidation of these alcohols appears to proceed via O-H, rather than C-H, bond cleavage.

The notion of O-H bond cleavage by **3** is supported by ^{1}H NMR analysis of the *tert*-butanol oxidation products under anaerobic conditions, revealing the formation of acetone (δ = 2.1) and 2-methylpropene (δ = 1.73, 6H; δ = 4.67, 2H) in respective yields of 50% and 40% (Table S7). Cleavage of the *t*-BuOH O-H bond should yield a *tert*-butoxyl radical that would readily decay to acetone via the well-documented β-scission pathway[22]. On the other hand, 2-methylpropene derives from acid-promoted dehydration of *t*-BuOH via *t*-butyl cation[23]. The protons needed for this transformation are generated in the course of bulk electrolysis from oxidation of the solvent as mentioned above. Unfortunately we cannot find an appropriate non-oxidizable base to neutralize these protons prior to substrate addition and not be readily oxidized by **3**. However, in support of our proposal, a comparable yield of 2-methylpropene (but no acetone) is observed when **3** is first reduced to **2** by 1 equiv ferrocene before the addition of *t*-BuOH.

Both alcohols have D_{O-H} values greater than 105 kcal mol^{-1} (105.2 and 106.3 kcal mol^{-1} for MeOH and *t*-BuOH)[24] and these O-H bonds are cleaved by **3** instead of the weaker C-H bonds in the molecule. Indeed on a per hydrogen basis, the O-H bond of *t*-BuOH is cleaved by **3** ~50 times faster than a C-H bond of cyclohexane, which has a D_{C-H} comparable to that of the C-H bonds of *t*-BuOH. Similarly, the O-H bond of MeOH reacts with **3** 10 times faster than a C-H bond of cyclooctane. Given the high redox potential of **3**, it may react by electron transfer from one of the nonbonding oxygen orbitals of the substrate, instead of a hydrogen atom transfer (HAT) process typically associated with C-H bond cleavage. However, having an oxygen atom in the substrate is apparently insufficient to trigger this alternative mechanism, because the oxidation rates of both THF and *tert*-butyl methyl ether (*t*-BME) fall nicely on the line correlating log k_2' and D_{C-H} (Fig. 5). We therefore propose that for alcohol oxidation proton transfer from the O-H group is coupled with the electron abstraction from the O atom. Such a

proton coupled electron transfer mechanism would be consistent with the observation of an O-H/O-D KIE that is smaller than for C-H bond cleavage (Fig. 6).

Complex **3** is thus unique among iron-based oxidants in its ability to cleave both strong C-H and O-H bonds. Table 2 compares rate constants for **3** and selected mononuclear oxoiron(IV) complexes. Complex **3** differs from the other complexes listed in the table in having a bridging oxo group instead of a terminal oxo group. Of note is the significantly larger second order rate constant for cyclohexane oxidation by **3** at 10 °C relative to those obtained at 25 °C for $[Fe^{IV}(O)(Bn\text{-}TPEN)]^{2+}$ and $[Fe^{IV}(O)(N4Py)]^{2+}$ [ref. [18]]. Even without accounting for the 15° temperature difference, **3** is still respectively over two and three orders of magnitude more effective at oxidizing cyclohexane than $[Fe^{IV}(O)(Bn\text{-}TPEN)]^{2+}$ and $[Fe^{IV}(O)(N4Py)]^{2+}$. The latter two complexes to date represent the most reactive of the oxoiron(IV) complexes that can be isolated or generated in high yield. This greater reactivity of **3** may derive from its much higher redox potential.

On the other hand, **3** appears less reactive than $[Fe^{IV}(O)(OH_2)_5]^{2+}$, a transient species trapped from the reaction of $[Fe^{II}(OH_2)_6]^{2+}$ and O_3 at pH 1 (Table 2)[25]. Due to its short half life, $[Fe^{IV}(O)(OH_2)_5]^{2+}$ has only been characterized by its UV and Mössbauer spectral properties[26]. Its $Fe^{IV/III}$ potential has been estimated to be comparable to that of **3** on the basis of its ability to oxidize Cl^- ion[27], but $[Fe^{IV}(O)(OH_2)_5]^{2+}$ reacts with CH_3CN more rapidly than **3** by a factor of more than two orders of magnitude. An important difference between **3** and $[Fe^{IV}(O)(OH_2)_5]^{2+}$ is the spin state of the individual iron centers, the former being $S = 1$ and the latter $S = 2$. A number of DFT calculations suggest that high-spin oxoiron(IV) centers have lower activation barriers for C-H bond cleavage[28–31], and the greater C-H bond cleavage activity of $[Fe^{IV}(O)(OH_2)_5]^{2+}$ supports this notion.

Complex **3** also differs from Fe=O complexes listed in Table 2 in its preference to cleave the O-H bonds of MeOH and *t*-BuOH, rather than their C-H bonds. This difference is starkly demonstrated by the observation of C-H/C-D kinetic isotope effects (KIE) of 4–8 for MeOH oxidation by the three oxoiron(IV) complexes[25,32] and its absence in the case of **3**. MeOH and *t*-BuOH oxidation by **3** instead exhibits a small but measurable O-H/O-D KIE. Why **3** should specifically target the O-H bond instead of the weaker C-H bonds of the alcohol is not clear and will be a subject for further investigation.

In conclusion, we have generated and characterized a novel diiron(IV) complex **3** with a redox potential +1.50 V vs. $Fc^{+/o}$, the highest $Fe^{IV/III}$ potential electrochemically determined to date[9,10,13,17,33–35]. This high potential suggests that **3** should be quite a powerful oxidant. Indeed **3** can cleave the strong C-H bonds of cyclohexane, while $[Fe^{IV}_2(\mu\text{-}O)_2(N4)_2]^{4+}$, a complex that serves as the synthetic precedent for the $Fe^{IV}_2(\mu\text{-}O)_2$ core proposed for MMO-**Q**[10] can only attack the weak C-H bonds of dihydroanthracene. Furthermore **3** reacts much faster with cyclohexane than mononuclear Fe^{IV}=O complexes of closely related ligands. Unexpectedly, we find that **3** preferentially cleaves the stronger O-H bonds of MeOH and *t*-BuOH instead of their C-H bonds, representing the first example of O-H bond activation for iron complexes. However, the cyclohexane oxidation rate of **3** is still orders of magnitude smaller than the methane oxidation rate of the diiron(IV) intermediate **Q** of MMO[36,37]. This reactivity gap may arise from a difference in the spin states of the individual iron centers in the complexes ($S = 1$ for **3** and $S = 2$ for **Q**). Complex **3** also differs from MMO-**Q** in the fact that it carries out substrate dehydrogenation rather than hydroxylation. From this perspective, the action of **3** more closely resembles that of fatty acid desaturases, which like MMO also have diiron active sites and are thus proposed to generate diiron(IV) oxidants in their catalytic cycle[38]. As discussed for **3** above, the difference in the reactivities of MMO and the fatty acid desaturases may hinge on the relative ease by which C-O bond formation between the incipient alkyl radical and the Fe-OH unit (i.e. oxygen rebound) can take place relative to electron

transfer between them[19–21], and the results for **3** can help us understand how different but related enzyme active sites can modulate the outcome of substrate oxidation. Lastly, our intriguing results demonstrate that complexes with very high $Fe^{IV/III}$ potential can be generated in high yield and characterized spectroscopically and set the stage for future efforts aimed at more efficient hydrocarbon oxidation by synthetic iron complexes.

Supplementary Material

Refer to Web version on PubMed Central for supplementary material.

Acknowledgments

This work was supported by NIH grants EB-001475 (E.M.), GM-38767 (L.Q.) and NIH Graduate Traineeship GM-08700 (E.R.F.). XAS data were collected on beamlines 7–3 and 9–3 at the Stanford Synchrotron Radiation Laboratory (SSRL), a national user facility operated by Stanford University on behalf of the U.S. Department of Energy, Office of Basic Energy Sciences. The SSRL Structural Molecular Biology Program is supported by the Department of Energy, Office of Biological and Environmental Research, and by the National Institutes of Health, National Center for Research Resources, and Biomedical Technology Program. We thank Drs. Matthew Latimer and Allyson Aranda for technical support and advice during XAS data collection. We also thank Dr. Victor G. Young, Jr. and the X-ray Crystallographic Laboratory of the University of Minnesota for expert assistance in the crystal structure determination.

References

1. Hanson RS, Hanson TE. Methanotrophic Bacteria. Microbiol Rev 1996;60:439–471. [PubMed: 8801441]
2. Wallar BJ, Lipscomb JD. Dioxygen Activation by Enzymes Containing Binuclear Non-Heme Iron Clusters. Chem Rev 1996;96:2625–2657. [PubMed: 11848839]
3. Merkx M, et al. Dioxygen Activation and Methane Hydroxylation by Soluble Methane Monooxygenase: A Tale of Two Irons and Three Proteins. Angew Chem Int Ed 2001;40:2782–2807.
4. Balasubramanian R, Rosenzweig AC. Structural and Mechanistic Insights into Methane Oxidation by Particulate Methane Monooxygenase. Acc Chem Res 2007;40:573–580. [PubMed: 17444606]
5. Lee SK, Fox BG, Froland WA, Lipscomb JD, Münck E. A Transient Intermediate of the Methane Monooxygenase Catalytic Cycle Containing an $Fe^{IV}Fe^{IV}$ Cluster. J Am Chem Soc 1993;115:6450–6451.
6. Liu KE, et al. Kinetic and Spectroscopic Characterization of Intermediates and Component Interactions in Reactions of Methane Monooxygenase from Methylococcus capsulatus (Bath). J Am Chem Soc 1995;117:10174–10185.
7. Nesheim JC, Lipscomb JD. Large Kinetic Isotope Effects in Methane Oxidation Catalyzed by Methane Monooxygenase: Evidence for C-H Bond Cleavage in a Reaction Cycle Intermediate. Biochemistry 1996;35:10240–10247. [PubMed: 8756490]
8. Shu L, et al. An $Fe^{IV}{}_2O_2$ Diamond Core Structure for the Key Intermediate Q of Methane Monooxygenase. Science 1997;275:515–518. [PubMed: 8999792]
9. Ghosh A, et al. Catalytically Active μ-Oxodiiron(IV) Oxidants from Iron(III) and Dioxygen. J Am Chem Soc 2005;127:2505–2513. [PubMed: 15725005]
10. Xue G, et al. A Synthetic Precedent for the $[Fe^{IV}{}_2(\mu\text{-}O)_2]$ Diamond Core Proposed for Methane Monooxygenase Intermediate Q. Proc Natl Acad Sci USA 2007;104:20713–20718. [PubMed: 18093922]
11. Xu JY, et al. Iron(III) complexes with the Ligand N′, N′-Bis[(2-pyridyl)-methyl]ethylenediamine (uns-penp) and Its Amide Derivative N-Acetyl-N′, N′-bis[(2-pyridyl)methyl]ethylenediamine (acetyl-uns-penp). Eur J Inorg Chem 2006:1601–1610.
12. Kurtz DM Jr . Oxo- and Hydroxo-Bridged Diiron Complexes: A Chemical Perspective on a Biological Unit. Chem Rev 1990;90:585–606.
13. Slep LD, et al. Mixed-Valent $\{Fe^{IV}(\mu\text{-}O)(\mu\text{-carboxylato})_2Fe^{III}\}^{3+}$ Core. J Am Chem Soc 2003;125:15554–15570. [PubMed: 14664603]

14. Norman RE, et al. (μ-Oxo)(μ-carboxylato)diiron(III) Complexes with Distinct Iron Sites. Consequences of the Inequivalence and Its Relevance to Dinuclear Iron-Oxo Proteins. J Am Chem Soc 1990;112:1554–1562.
15. Jackson TA, et al. Axial Ligand Effects on the Geometric and Electronic Structures of Nonheme Oxoiron(IV) Complexes. J Am Chem Soc 2008;130:12394–12407. [PubMed: 18712873]
16. Rohde JU, et al. Nonheme Oxoiron(IV) Complexes of Tris(2-pyridylmethyl)amine with *cis*-Monoanionic Ligands. Inorg Chem 2006;45:6435–6445. [PubMed: 16878956]
17. Collins MJ, Ray K, Que L Jr. Electrochemical Generation of a Nonheme Oxoiron(IV) Complex. Inorg Chem 2006;45:8009–8011. [PubMed: 16999397]
18. Kaizer J, et al. Nonheme $Fe^{IV}O$ Complexes That Can Oxidize the C-H Bonds of Cyclohexane at Room Temperature. J Am Chem Soc 2004;126:472–473. [PubMed: 14719937]
19. Kumar D, de Visser SP, Sharma PK, Cohen S, Shaik S. Radical Clock Substrates, Their C-H Hydroxylation Mechanism by Cytochrome P450, and Other Reactivity Patterns: What Does Theory Reveal about the Clocks' Behavior? J Am Chem Soc 2004;126:1907–1920. [PubMed: 14871124]
20. Kumar D, de Visser SP, Shaik S. Oxygen Economy of Cytochrome P450: What Is the Origin of the Mixed Functionality as a Dehydrogenase-Oxidase Enzyme Compared with Its Normal Function? J Am Chem Soc 2004;126:5072–5073. [PubMed: 15099082]
21. Jin Y, Lipscomb JD. Desaturation reactions catalyzed by soluble methane monooxygenase. J Biol Inorg Chem 2001;6:717–725. [PubMed: 11681705]
22. Griller D, Ingold KU. Free-Radical Clocks. Acc Chem Res 1980;13:317–323.
23. Vollhardt, KPC. Organic Chemistry. W. H. Freeman and Company; New York: 1987. The Reactions of Alcohols and the Chemistry of Ethers; p. 308-358.
24. Luo, YR. Comprehensive Handbook of Chemical Bond Energies. Taylor & Francis; Boca Raton: 2007. BDEs of O-X bonds; p. 255-369.
25. Pestovsky O, Bakac A. Reactivity of Aqueous Fe(IV) in Hydride and Hydrogen Atom Transfer Reactions. J Am Chem Soc 2004;126:13757–13764. [PubMed: 15493935]
26. Pestovsky O, et al. Aqueous Fe^{IV}=O: Spectroscopic Identification and Oxo Group Exchange. Angew Chem Int Ed 2005;44:6871–6874.
27. Jacobsen F, Holcman J, Sehested K. Reactions of the Ferryl Ion with Some Compounds Found in Cloud Water. Int J Chem Kinet 1998;30:215–221.
28. Shaik S, Hirao H, Kumar D. Reactivity of High-Valent Iron-Oxo Species in Enzymes and Synthetic Reagents: A Tale of Many States. Acc Chem Res 2007;40:532–542. [PubMed: 17488054]
29. Sastri CV, et al. Axial ligand tuning of a nonheme iron(IV)-oxo unit for hydrogen atom abstraction. Proc Natl Acad Sci USA 2007;104:19181–19186. [PubMed: 18048327]
30. Decker A, et al. Spectroscopic and Quantum Chemical Studies on Low-Spin FeIV=O Complexes: Fe-O Bonding and Its Contributions to Reactivity. J Am Chem Soc 2007;129:15983–15996. [PubMed: 18052249]
31. Bernasconi L, Louwerse MJ, Baerends EJ. The Role of Equatorial and Axial Ligands in Promoting the Activity of Non-Heme Oxidoiron(IV) Catalysts in Alkane Hydroxylation. Eur J Inorg Chem 2007:3023–3033.
32. Klinker, EJ. Ph.D thesis. University of Minnesota-Twin Cities; Minneapolis: 2007.
33. Berben, LA.; Peters, JC. Inorg Chem. ASAP; 2008. Dimanganese and Diiron Complexes of a Binucleating Cyclam Ligand: Four-Electron, Reversible Oxidation Chemistry at High Potentials.
34. Berry JF, Bill E, Bothe E, Neese F, Wieghardt K. Octahedral Non-Heme Oxo and Non-Oxo Fe(IV) Complexes: An Experimental/Theoretical Comparison. J Am Chem Soc 2006;128:13515–13528. [PubMed: 17031965]
35. Zheng H, Yoo SJ, Münck E, Que L Jr. The Flexible $Fe_2(\mu\text{-}O)_2$ Diamond Core: A Terminal Iron(IV)-Oxo Species Generated from the Oxidation of a Bis(μ-oxo)diiron(III) Complex. J Am Chem Soc 2000;122:3789–3790.
36. Brazeau BJ, Lipscomb JD. Kinetics and Thermodynamics of Methane Monooxygenase Compound Q Formation and Reaction with Substrates. Biochemistry 2000;39:13503–13515. [PubMed: 11063587]

37. Valentine AM, Stahl SS, Lippard SJ. Mechanistic Studies of the Reaction of Reduced Methane Monooxgyenase Hydroxylase with Dioxygen and Substrates. J Am Chem Soc 1999;121:3876–3887.

38. Fox BG, Lyle KS, Rogge CE. Reactions of the Diiron Enzyme Stearoyl-Acyl Carrier Protein Desaturase. Acc Chem Res 2004;37:421–429. [PubMed: 15260504]

39. Luo, YR. Comprehensive Handbook of Chemical Bond Energies. Taylor & Francis; Boca Raton: 2007. BDEs of C-H bonds; p. 19-147.

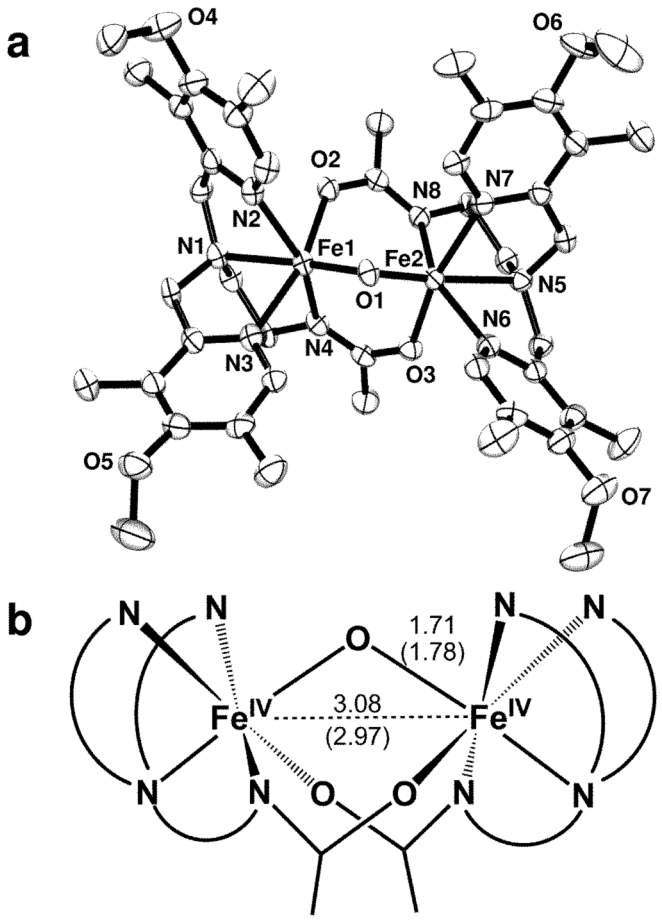

Fig. 1.

The structures of complexes **1** and **3**. (a) ORTEP plot of $[Fe^{III}_2O(L)_2]^{2+}$ (**1**) with thermal ellipsoids drawn at the 50% probability level. Carbon atoms shown are not labeled, and hydrogen atoms are omitted for clarity. Selected distances and angles: Fe1-O1: 1.795(16) Å; Fe1-O2: 2.007(16) Å; Fe1-N1: 2.237(2) Å; Fe1-N2, N3: 2.157(2) Å; Fe1-N4: 2.088(2) Å; Fe1-Fe2: 3.007(3) Å; Fe1-O1-Fe2: 113.68(8)°. (b) Schematic representation of the structure of **3** with labeled Fe-Fe and Fe-O distances determined by EXAFS analysis. Numbers shown in parentheses are the corresponding distances of **1** (see also Table 1).

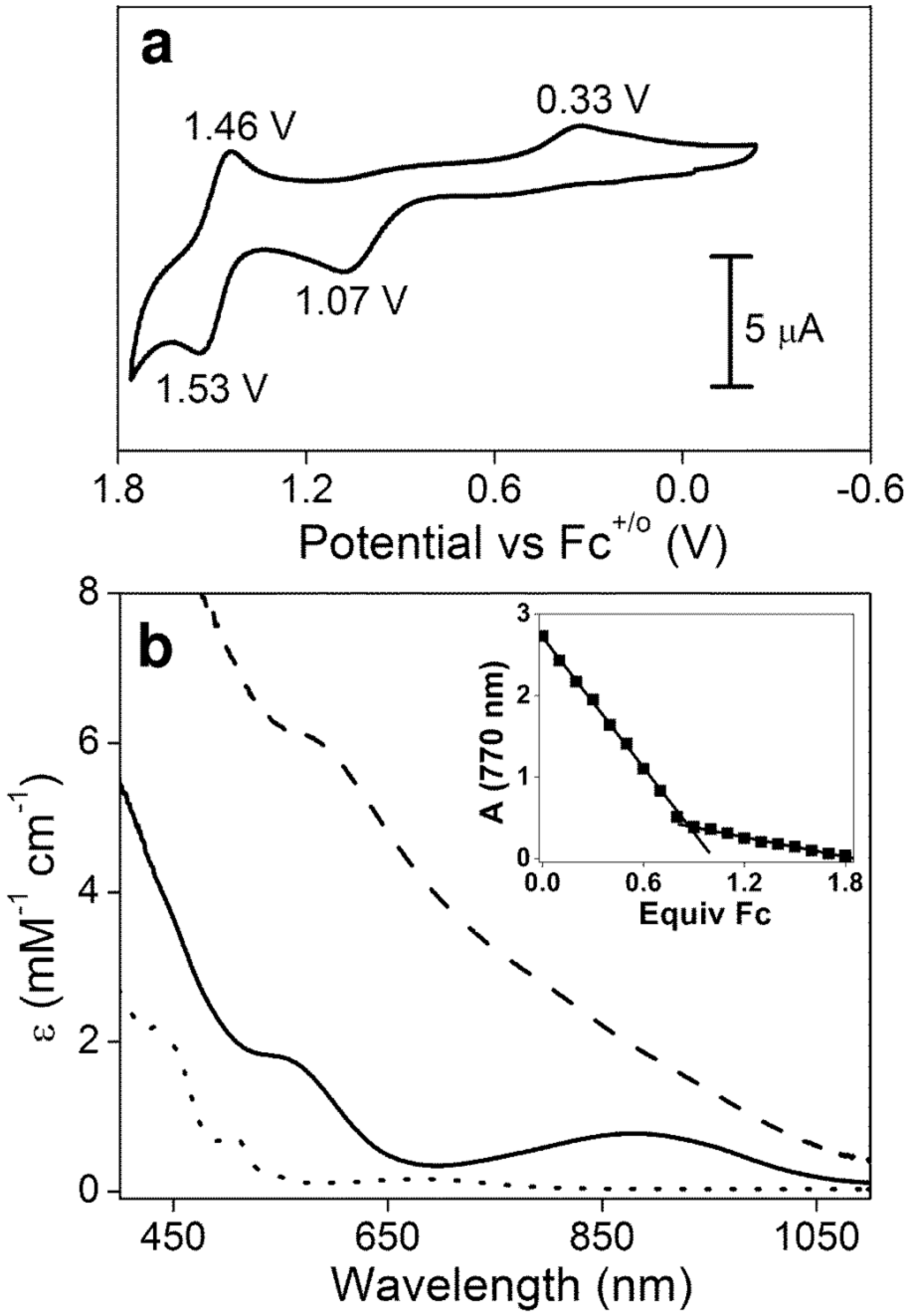

Fig. 2.

Characterization of complexes **1**, **2** and **3**. (a) Cyclic voltammetry of **1** in CH_3CN at room temperature with 0.10 M KPF_6 as the supporting electrolyte at a scan rate of 100 mV s^{-1}. Peak potentials are shown next to each peak. (b) UV/visible spectra of the Fe^{III}-O-Fe^{III} complex **1** (dotted line), the Fe^{III}-O-Fe^{IV} species **2** (solid line) and the Fe^{IV}-O-Fe^{IV} complex **3** (dashed line) taken in CD_3CN at −40 °C. Inset: ferrocene titration of 1 mM **3** monitored at 770 nm.

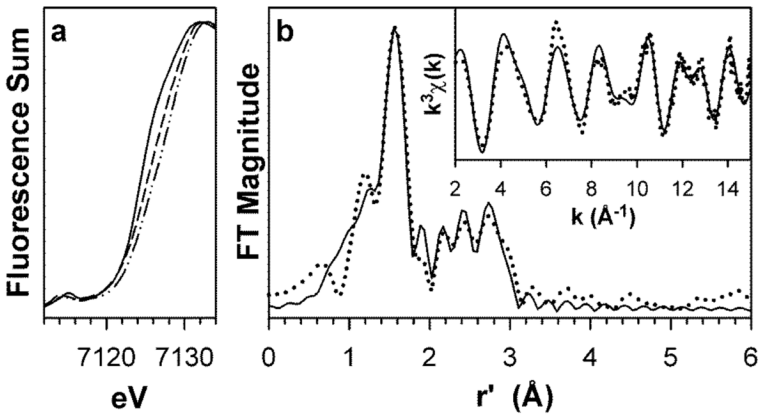

Fig. 3.

X-ray absorption spectra of complexes **1**, **2** and **3**. (a) X-ray absorption edge spectra of **1** (——), **2** (– – –), and **3** (–··–··–), showing the blue-shift of the Fe K-edge transition with progressive oxidation of the iron centers. (b) Fourier transform of the Fe K-edge EXAFS data ($k^3\chi(k)$) and unfiltered EXAFS spectra ($k^3\chi(k)$, inset) of **3**. Experimental data is shown with dotted (·····) lines and fits with solid (——) lines. Fourier transformation range, k = 2.0 – 15.0 $Å^{-1}$. Fit parameters are shown in bold italics in Table S4 of the Supplementary Information.

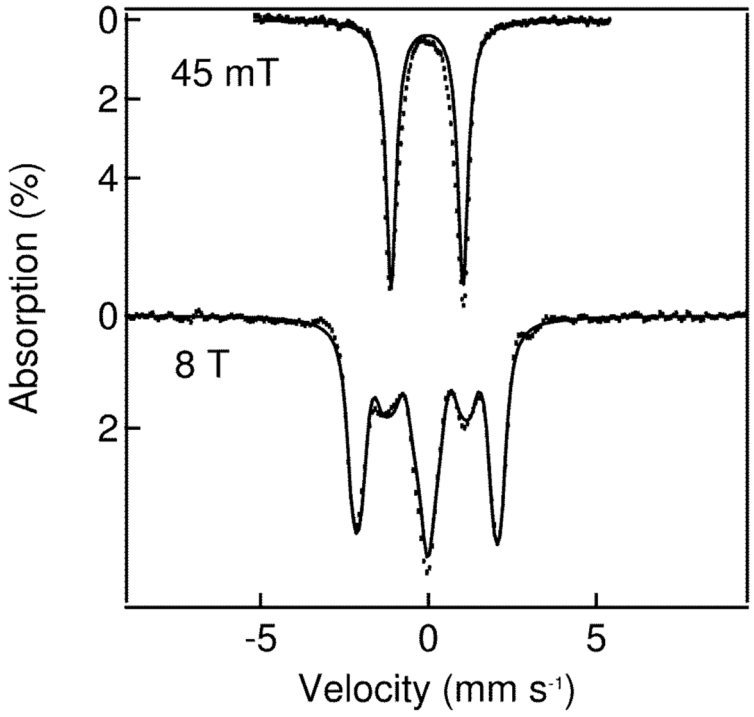

Fig. 4.

4.2 K Mössbauer spectra of **3**. Dotted lines represent experimental data points, while the solid lines are spectral simulations assuming an $S = 0$ ground state and two equivalent Fe sites with $\delta = -0.05$ mm s^{-1}, $\Delta E_Q = 2.14$ mm s^{-1} and (asymmetry parameter) $\eta = 0.9$.

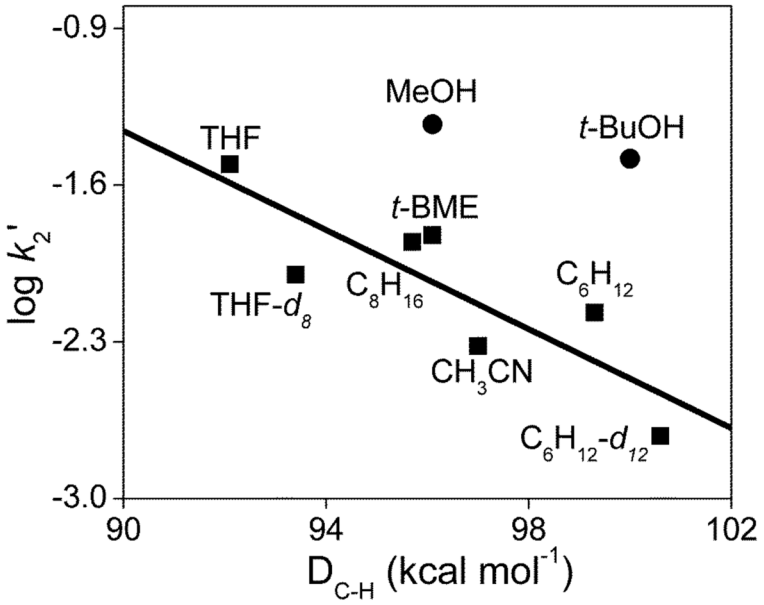

Fig. 5.

Oxidative reactivity study of **3** in CD_3CN at 10 °C. The solid line represents the best linear fit correlating the log k_2' values for the reactions of hydrocarbons with **3** (■) with their C-H bond dissociation energies. k_2' is the normalized second order rate constant (second order rate constant k_2 divided by the number of equivalent C-H bonds on the substrate that may be attacked by **3**). For MeOH and *t*-BuOH, the filled circles (●) represent the values assuming that a C-H bond is attacked. D_{C-H} values were obtained from refs [18, 24] and [39].

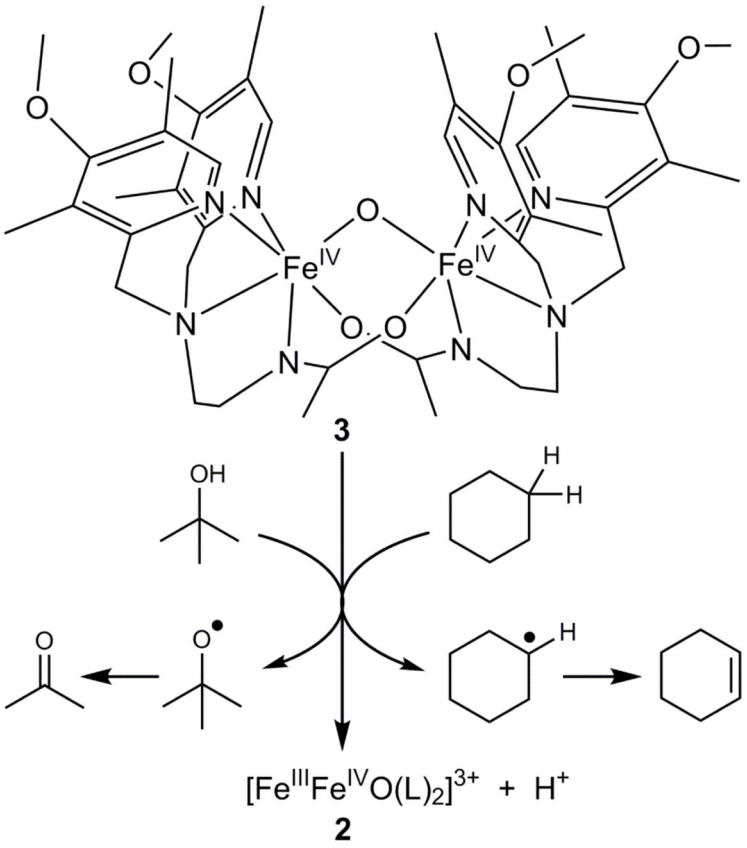

Fig. 6.

Reaction scheme of **3** in its oxidation of cyclohexane and *t*-butanol. Complex **3** acts as a one-electron oxidant that cleaves a C-H bond of cyclohexane and the O-H bond of *t*-butanol.

Table 1

XAS and Mössbauer data for $[Fe_2O(L)_2]^{n+}$

	Edge energy, eV	r(Fe-μ-O), Å	r(Fe-N), Å	r(Fe-C), Å	r(Fe-Fe), Å	δ, mm s^{-1}	ΔE_Q, mm s^{-1}
1	7124.1	1.78	2.11	3.07	2.97	0.45	1.30
2	7124.9	1.70	1.96	2.89	3.07	0.07[a]	1.57
3	7125.6	1.71	1.96	2.88	3.08	−0.05	2.14

[a]Complex **2** is a valence-delocalized $Fe^{III}Fe^{IV}$ complex that yields one doublet with δ = 0.07 mm s^{-1} at 120 K; a more detailed description of this interesting complex will be presented in a future publication.

Table 2

Second order rate constants (M^{-1} s^{-1}) for the reactions of iron(IV) complexes. Values in brackets represent KIE values where available

Complexes[a]	$E_{1/2}$ ($Fe^{IV/III}$) (vs. $Fc^{+/0}$)	Fe Spin State	*c*-C_6H_{12}	CH_3CN	MeOH	*t*-BuOH	Ref
3 (10 °C)	1.50	*S* = 1	0.081 [C-H, 3.5]	0.014	0.14 [O-H, 1.5]	0.30 [O-H, 1.4]	this work
$[Fe(O)(Bn\text{-}TPEN)]^{2+}$ (25 °C)	1.07	*S* = 1	3.9×10^{-4}	2×10^{-6} [b] [C-H, 4]	2.8×10^{-3} [c] [C-H, 8]	N.A.	18, 32
$[Fe(O)(N4Py)]^{2+}$ (25 °C)	0.90	*S* = 1	5.5×10^{-5}	2×10^{-7} [b]	4.4×10^{-4} [c] [C-H, 7]	N.A.	17, 18,
$[Fe(O)(OH_2)_5]^{2+}$ (25 °C)	~1.4[d]	*S* = 2	N.A.[e]	4.1 [C-H, 4.1]	572 [C-H, 4.4]	60	25, 27
MMO-**Q** (25 °C)	N.A.	*S* = 2	$3\sim4 \times 10^4$ for CH_4				36, 37

[a] Bn-TPEN = *N*-benzyl-*N*, *N*′, *N*′-tris(2-pyridylmethyl)-1,2-diaminoethane N4Py = *N*, *N*-bis(2-pyridylmethyl)-bis(2-pyridyl)methylamine

[b] Estimated from $t_{1/2}$ values in acetonitrile solvent from ref. 18 or 32.

[c] Data obtained at 40 °C from ref. 32.

[d] It has not been possible to establish the $Fe^{IV/III}$ potential for $[Fe(O)(OH_2)_5]^{2+}$ by electrochemical means due to its very short lifetime; the value given in the table is an estimate from ref. 27 based on its ability to oxidize Cl^- ion.

[e] No oxidation rate for cyclohexane or any other hydrocarbon has been reported due to the immiscibility of such substrates with the aqueous medium in which $[Fe(O)(OH_2)_5]^{2+}$ is generated.